The atomic environment and valence state of Ce implanted in Y_2O_3

1999 J. Phys.: Condens. Matter 11 1225

(http://iopscience.iop.org/0953-8984/11/5/010)

J. Phys.: Condens. Matter **11** (1999) 1225–1234. Printed in the UK PII: S0953-8984(99)96758-9

The atomic environment and valence state of Ce implanted in Y_2O_3

Agnès Traverse†‖, Annick Quivy‡ and François Jollet§¶

† Laboratoire pour l'Utilisation du Rayonnement Electromagnétique, Université Paris-Sud, Bâtiment 209 A, BP 34, 91898 Campus Orsay, France
‡ Centre d'Etudes de Chimie Métallurgie, CNRS, 15 rue G Urbain, 94407 Vitry Cédex, France
§ CEA, DSM/DRECAM/SRSIM, Bâtiment 462, CE Saclay, 91191 Gif-sur-Yvette Cédex, France

Received 14 August 1998, in final form 17 November 1998

Abstract. Ce ions were implanted in Y_2O_3. Via x-ray absorption spectroscopy, Ce was found to occupy the Y site, and to be surrounded by oxygen atoms. However, contrary to what one would expect on the basis of this substitution, the oxidation state was not purely trivalent. Thanks to the Anderson impurity model, it was possible to interpret the x-ray absorption features near the edge. Ce is found in an intermediate charge state resulting from the interaction of the f state with the valence band of Y_2O_3.

1. Introduction

By means of ion implantation, it is possible to introduce impurities in matrices. In ceramics, the site occupied by the impurity mainly depends (a) on the charge of the site as compared to the positive or negative character of the impurity, and (b) on the possible chemical bonds between the impurity and the neighbouring atoms in the occupied site. For example, in the AlN matrix, implanted Ti ions occupy the Al site [1], and hence are surrounded by N atoms, the heat of formation, ΔH, of TiN being -80 kcal mol^{-1}, more negative than that of AlN, -76.1 kcal mol^{-1} [2]. On the other hand, implanted copper ions do not occupy lattice sites, and thus form clusters for two reasons [3]: the Cu–N bonds are not thermodynamically favoured ($\Delta H_{Cu_3N} = 17.8$ kcal mol^{-1}) [2], and hence the Al site is forbidden and Cu (a positive ion) cannot occupy a N negative site. In metallic oxide matrices, MO_x, implanted metallic impurities usually occupy sites surrounded by O atoms [4, 5].

This ability of the implantation technique to introduce an impurity at a preferred site can be used to study specific oxygen environments of metallic atoms, varying the coordination number and the distance to the O shell. This might be especially interesting in the case of Ce, for which the participation of f electrons in the chemical bonding is still under study.

The matrix in which we chose to implant Ce is Y_2O_3. Several reasons guided the matrix choice. The electronic structure of Y_2O_3 is already experimentally and theoretically well known [6]. It can be calculated in a one-electron approximation using a self-consistent tight-binding method. We have already performed an implantation of Zr in Y_2O_3, and Zr was found to occupy the Y site [7]. If Ce occupies such sites, its expected oxidation state is a

‖ Author to whom any correspondence should be addressed. E-mail: traverse@lure.u-psud.fr; fax: 33 1 6446 7497.
¶ Now at: CEA, Centre d'Etudes de Bruyères le Châtel, BP12, F-91680 Bruyères le Châtel, France.

0953-8984/99/051225+10$19.50

trivalent one, like that of Y. However, a study was performed on CeO_2-doped Y_2O_3 wherein Ce was found to be surrounded by eight oxygen atoms instead of six oxygen atoms as around Y [8]. In this environment, Ce is tetravalent, but some differences in the intensities and peak energy separations in the L_3 absorption edge appear as compared to the case for CeO_2. They were qualitatively explained by an increase of the charge transfer in the initial state due to the increase of the Madelung field as a consequence of the change in the mean Ce–O distance. Hence it appears that the Ce tetravalent state is more favoured than the trivalent one in such a system, and that to be in this oxidation state, Ce must be able to trap the required number of O atoms.

In this work, the samples were prepared by Ce implantation in Y_2O_3. Several techniques were combined to characterize them. The Ce content and its implantation profile in Y_2O_3 were measured by Rutherford backscattering (RBS). X-ray diffraction (XRD) allowed us to obtain the lattice parameter of Y_2O_3 and of CeO_2 used as a standard sample. The main goal of this work was to obtain information about the local atomic and electronic environment around Ce and Y. Hence the x-ray absorption technique was used, recording both extended x-ray absorption fine structure (EXAFS) and x-ray absorption near-edge structure (XANES) at the K edge of Y and the L_3 edge of Ce. Ce atoms were found to occupy Y sites, leading to a mean coordination number of six O atoms located at a distance of 0.235 nm. However, contrary to expectation for a Y substitution site, the cerium valence is not purely trivalent. Using the Anderson impurity model, it was possible to reproduce the experimental L_3 edge of Ce, which is found in an intermediate charge state between 3+ and 4+.

2. Experimental procedure

2.1. Sample preparation

Pure powder (5N, Rhône-Poulenc, France) of Y_2O_3 was sintered under hot isostatic pressure (HIP): 150 MPa at 1450 °C for 45 min. After HIP processing, slices that were 1 mm thick were cut, mechanically polished, and then annealed for two hours in air at 1500 °C to remove oxygen vacancies and residual stresses.

Three sintered Y_2O_3 samples were simultaneously implanted with 3×10^{16} Ce ions cm^{-2} at 200 keV and 300 K [9]. The ion current was maintained at 0.8 μA cm^{-2} to avoid target heating. For such implantation conditions, the TRIM code [10] calculates a projected range of 54.5 nm and a FWHM (full width at half-maximum) of 49 nm. The TRIM code also provides the amount of energy density which is deposited in the matrix when the implanted ions trace out their paths. Under the Ce-implantation conditions, the energy density transmitted to the matrix atoms is 14.6 keV nm^{-1}.

In the following, the sample studied in this work will be denoted as 'Y_2O_3/Ce-impl.' whereas the sample of reference [8] will be denoted as 'Y_2O_3/Ce-dop.'.

2.2. Sample characterization

For sample characterization via RBS and XAS, it was necessary to cover the surfaces of the samples (implanted or non-implanted) with 5 nm carbon layers in order to avoid charge problems.

The RBS analysis was performed using He^{2+} particles of 2.8 MeV with a current of 20 nA and a total fluence of 10 μC per sample [11]. The He incident energy was chosen such as to separate the Ce peak from the Y signal so that the actual amount of Ce in the sample can be deduced from the peak area compared to a standard.

An x-ray absorption investigation was performed on the D42 station of the DCI storage ring (LURE) equipped with a Si331 monochromator. EXAFS spectra were recorded at the Y K edge (17 038 eV) for an implanted and for a non-implanted sample from 16 850 eV to 17 950 eV, with 2 eV steps, for two seconds. At the Ce L_3 edge (5724 eV), we performed both EXAFS (from 5660 eV to 6150 eV, with 1 eV steps) and XANES (5700 eV to 5800 eV, with 0.5 eV steps) measurements. Special care was taken in checking that in the energy region near 5700 eV, no contamination of the spectra due to the presence of harmonics occurred. The first ionization chamber, where the incident photon intensity was measured, was partially filled with air. As the matrix is implanted, and thus modified, on a layer of thickness about 80 nm, the total-electron-yield mode was used, instead of the transmission mode, the escaping electron depth being of the same order of magnitude as that of the Ce-implanted layer. Standard samples of compacted Y_2O_3 powder, of metallic Ce (made of a Ce layer covered by a Fe layer to avoid oxidation), of CeO_2 where Ce is in the Ce^{4+} state, and of Ce pentanitrate $Ce(NO_3)_5[(C_6H_5)_3C_2H_2P]$ where Ce is in the Ce^{3+} state were also measured via XAS for comparison purposes.

The background was subtracted from the XANES spectra, and then they were normalized at the energy value of 5785 eV.

The background was subtracted from the EXAFS spectra. After subtraction of the atomic absorption, the oscillations were extracted, then the spectra were Fourier transformed to provide a pseudoradial function [12]. The k-range for the Fourier transformation was 26.5 nm^{-1} to 130 nm^{-1} at the Y K edge of Y_2O_3 and 25 nm^{-1} to 100 nm^{-1} at the Ce L_3 edges of CeO_2 and Y_2O_3/Ce-impl. This limitation in the k-range arises from the occurrence of the Ce L_2 edge at 6165 eV. The first peak corresponding to the oxygen shell around the cation was then filtered and back-Fourier-transformed. Fitting of these back-Fourier-transformed spectra provides quantitative information about the local environment of the probed atom, i.e. the number of O neighbours and the distances of the neighbouring shells. The filtered oscillations were fitted using the phase shift and scattering amplitude for the cation–oxygen contributions deduced from the FEFF code [13]. The uncertainties in the number of neighbours, N, are typically $\pm 10\%$, whereas the distances, R, are given ± 0.002 nm. We recall that the FEFF code calculates an x-ray absorption coefficient, using a multiple-scattering approach and a curved-wave formalism. A cluster of atoms is built. Given the atomic charge densities and atomic potentials, the scattering muffin-tin potentials are constructed, taking into account renormalization, overlap, and self-consistency. From these muffin-tin potentials, phase shifts and effective scattering amplitudes are calculated. Details on the FEFF calculations that we

Table 1. Structural results from XRD and XAS investigations. In the case of pentanitrate, superscript a indicates our experimental result, while superscript b indicates results from reference [14]. a is the lattice parameter, N is the number of neighbours, R is the distance between the cation and O atoms, and σ is the Debye–Waller factor, representative of thermal and structural disorder.

	X-ray diffraction		X-ray absorption		
Sample	a (nm)	$R_{\text{cation}-\text{O}}$ (nm)	O shell N	O shell σ (nm)	O shell R (nm)
Pentanitrate			10.5[a] 10[b]	0.0085	0.257[a] 0.257[b]
CeO_2	0.5393	0.2335	8	0.0066	0.232
Y_2O_3, non-implanted	1.0597	0.2278	6	0.0079	0.226
Y_2O_3, implanted	1.0590	0.2277	6	0.0079	0.225
Ce in Y_2O_3/Ce-impl.			6	0.0081	0.235

have performed are given in the next section.

Diffraction spectra were recorded using Co K$\alpha_1\alpha_2$ x-rays irradiating compacted Y_2O_3 powder, non-implanted and Ce-implanted Y_2O_3 samples, and the CeO_2 sample. The pentanitrate is expected to be organized as follows: ten O atoms around Ce at a distance of 0.257 nm, as reported in table 1 [14].

Which depths are analysed depends on the investigation technique. X-ray diffraction probes several microns—a thicker depth than the implantation one. In the XAS experiments performed at the K edge of Zr, a thickness of about 200 nm is probed—about double the implanted-zone depth—whereas a thickness of about 60 nm is probed—slightly smaller than the implanted depth—in the XAS experiments performed at the L_3 edge of Ce.

3. Results

3.1. The composition and structural state of the Y_2O_3 matrix

The RBS spectrum allows us to measure a level of Ce of $(3.2 \pm 0.3) \times 10^{16}$ atoms cm^{-2} in the target, in agreement, within the experimental uncertainty, with the implanted fluence. Using the RUMP code [15] to fit the RBS spectrum, we obtain a Ce profile centred at 46 nm, whereas the FWHM is 67.5 nm. This leads to an average composition of $Y_2O_3Ce_{0.35}$ in the implanted zone. The number of Ce atoms divided by the total number of cations is thus 15%, close to the highest concentration reached in the Y_2O_3/Ce-dop. system, namely 13% [8].

Diffraction patterns display the typical cubic bixbyite well crystallized structure of Y_2O_3. As in the case of Y_2O_3 implanted with Zr [7], a partial modification of the crystalline cubic structure to a tetragonal form is observed. Lattice parameters deduced from diffraction patterns are reported in table 1. No increase in background is seen as due to amorphization of the implanted zone. But we recall that the depth probed is larger than the implanted depth.

From XAS at the Y K edge, we obtain the pseudoradial function (PRF) for around Y. The similarity of the PRFs before and after implantation (see figure 2, later) is proof that order around Y is retained over 0.8 nm and that no amorphization has occurred. The numbers of O neighbours and distances deduced from the treatment of the EXAFS oscillations are presented in table 1 for the non-implanted matrix and the implanted matrix.

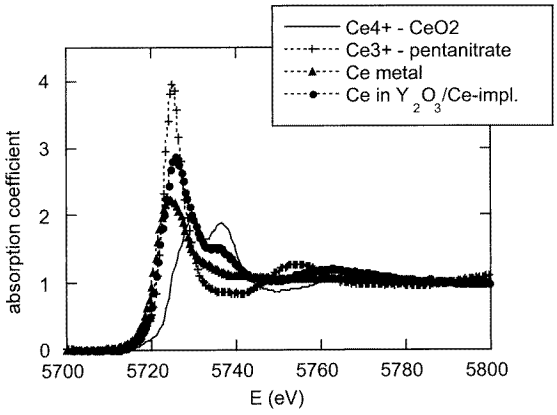

Figure 1. XANES spectra for CeO_2 (Ce^{4+} oxidation state), pentanitrate (Ce^{3+} oxidation state), metallic Ce, and Ce in Y_2O_3/Ce-impl.

3.2. The oxidation state of the implanted impurity

The two different oxidation states present in the CeO_2 and Ce pentanitrate samples are clearly observed in figure 1. The Ce^{4+} edge is shifted by about 6 eV from the Ce^{3+} edge. It displays two structures separated by 6.3 eV, in agreement with previous results [16], while only one peak is seen for the Ce^{3+} sample [14]. For comparison we plot the Ce-metal edge, located at the same energy as that of trivalent Ce, with only one peak of much lower intensity. Superimposed is the edge of Ce in Y_2O_3/Ce-impl., located between the edges of Ce metal and of oxides. A main peak is present with a shoulder at higher energy. From these plots, it is clear that the Ce implanted in Y_2O_3

(a) has a local environment different from that of CeO_2, and
(b) is neither in the Ce^{4+} nor in the Ce^{3+} pure oxidation state.

In addition, the fact that the edge of implanted Ce is different from that of Ce metal allowed us to conclude that Ce has not precipitated in the form of metallic clusters. The most probable site is thus a site surrounded by oxygen atoms. The EXAFS oscillations will give us more detailed information.

3.3. The implanted impurity site

3.3.1. Calculations from the FEFF code. We first calculated the absorption coefficient for Y_2O_3, at the Y K edge, taking into account the two different sites of Y in the bixbyite structure. The structural parameters used for the FEFF calculation are given in table 2: the space group, the lattice parameter, and the atom positions for O and the two Y types. 24 Y atoms (referred to as Y2 in table 2) are surrounded by two oxygen atoms located at 0.2249 nm, two O at 0.2278 nm, and two O at 0.2336 nm—hence there are six O at a mean distance of 0.2287 nm. Eight Y atoms (referred to as Y1 in table 2) are surrounded by six O atoms located at 0.2261 nm. There are two vacant sites around each type of Y atom. As the Debye temperature, Θ_D, of Y_2O_3 is not precisely known, we accounted for the thermal disorder (which appears through a Debye–Waller factor σ) by introducing $\Theta_D = 650$ K, a value chosen to adjust the calculated amplitude of the first peak in the pseudoradial function more or less to the experimental one. The parameter n_{leg}, which represents the number of paths allowed in the multiple-scattering approach used in the FEFF calculation, was fixed at 8 and the maximum length of the paths explored was 0.7 nm. The calculated oscillations were Fourier transformed over the same k-range as the experimental ones. The calculated and experimental pseudoradial functions are compared in figure 2, where a very good agreement is observed at least up to $R = 0.4$ nm for the number and position of the peaks. The first peak represents the O shell around Y, whereas the second double peak represents the second shell containing Y atoms and the third shell containing O atoms. A better agreement between the calculated and experimental pseudoradial functions for the whole R-range requires a fitting of a large number of parameters, and is beyond the scope of this paper.

Table 2. Structural parameters introduced in the FEFF calculation for Y_2O_3.

		Atom position				
	Space group		x	y	z	Lattice parameter
Y_2O_3	$IA3$	Y1 (8 atoms)	0.25	0.25	0.25	$a = 1.0604$ nm
		Y2 (24 atoms)	−0.314	0.0	0.25	
		O	0.389	0.15	0.377	

As the most probable site for implanted Ce is a Y substitutional site, the FEFF calculation was redone locating the Ce atom as the central one, taking into account again the two Y sites. The calculation was performed at the L_3 edge of Ce. Nothing else was changed in the input file for the calculation—neither the lattice parameter nor the Debye temperature. The pseudoradial function obtained by Fourier transformation of the EXAFS oscillations over the same k-range as for the experimental ones is compared to the experimental one in figure 3. The agreement is rather good. In particular, the occurrence of a single peak in the range 0.25 nm to 0.4 nm in the pseudoradial function of Ce in Y_2O_3/Ce-impl. instead of a double peak in the pseudoradial function of Y in Y_2O_3 is well reproduced. This change could be attributed to the modification in the absorbing atom potential, the only new parameter in the calculation. The amplitude difference might be due to a supplementary disorder in the system, induced by Ce implantation. There is also a shift in the x-axis between calculated and experimental pseudoradial functions, indicating that distances between implanted Ce ions and neighbouring shells have increased—an increase not taken into account *a priori* in the calculation—which is related to the larger size of the Ce ion as compared to Y.

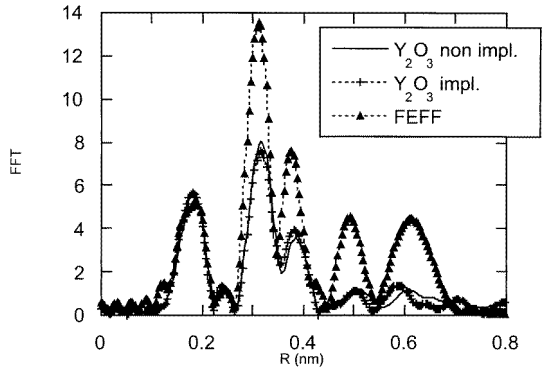

Figure 2. Comparison of the experimental pseudoradial functions for Y_2O_3 before and after Ce implantation and calculated by the FEFF code. The parameters for the calculation are given in table 2.

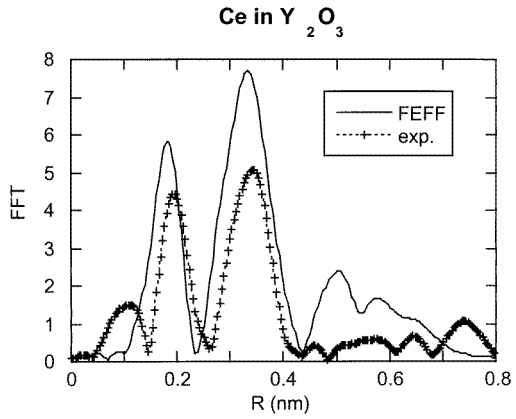

Figure 3. Comparison of the experimental pseudoradial functions and those calculated by the FEFF code for Ce in Y_2O_3/Ce-impl.

3.3.2. Results from simulations. Using the phases and amplitudes delivered by FEFF for Y–O and Ce–O, we have fitted the oscillations resulting from the filters on the pseudoradial functions of CeO_2, pentanitrate, Y_2O_3, and Ce in Y_2O_3/Ce-impl. The results are reported in table 1. For the pentanitrate, the expected oxygen surrounding is found. For Y_2O_3 and CeO_2, the distances are in agreement within the experimental uncertainty with the diffraction data.

Around Ce in Y_2O_3/Ce-impl., six O neighbours are found, as around Y, instead of eight, as around Ce in CeO_2. The Ce–O distance (0.2350 nm) is larger than the Y–O distance (0.226 nm) and similar to the Ce–O one in CeO_2 (0.2335 nm). This increase is in agreement with what was observed in figure 3.

4. Interpretation and discussion

4.1. The effect of Ce implantation in Y_2O_3

After implantation, the matrix is still well crystallized, as seen from the XRD pattern and the pseudoradial function deduced from the EXAFS data. No amorphization occurs under Ce-implantation conditions: 300 K and 14.6 keV nm^{-1} deposited in the matrix, a result which had already been found in the case of 300 K Zr implantation with 9.9 keV nm^{-1} deposited in the matrix. Yttria appears to be very resistant to implantation-induced disorder, as indeed are Al_2O_3 [17] and AlN [18] under similar conditions.

In Zr-implanted Y_2O_3, the tetragonalization of the matrix, as 'seen' by XRD, was interpreted as due to O loss (measured by nuclear reaction over O atoms) associated with ordering of the O vacancies [7]. This O loss results from Y–O bonds breaking inside the defect cascades, which is induced by energy deposition, followed by O–O bond formation and O_2 desorption. Although we did not measure the O content in Ce-implanted Y_2O_3, we interpret the similar XRD pattern modification as due to the tetragonalization of the matrix, induced by O loss. Oxygen reduction of implanted yttria is thus due to two factors:

(a) supplementary cations are introduced, and

(b) implantation induces O desorption.

4.2. The Ce site

Implanted Ce occupies the Y site, as Zr did [7]. The atomic arrangement around Ce is well ordered on a scale at least of the order of 0.4 nm, as indicated by the presence of a well defined peak located at about 0.36 nm in the pseudoradial function, representing a second shell of Y atoms and a third shell with O atoms. This is different from what was seen in the case of Zr implanted either in Y_2O_3 [7] or in Al_2O_3 [17], around which a high level of disorder was observed. Looking at the phase diagrams [2], a very crude and qualitative explanation might be found in the fact that the Zr-metal bonds are not so strong as the Ce-metal ones. Hence, even if Y substitution occurred because Zr–O and Ce–O bonds are favoured, on a larger scale structural order can only take place in the Ce case.

The average coordination number is the same around Y and implanted Ce: six O atoms, whereas the cation distance is slightly increased, 0.235 nm instead of 0.226 nm. For a very similar Ce concentration, a different atomic arrangement was found in Y_2O_3/Ce-dop. [8]: a coordination number of 8 and a distance of 0.228 nm. As a consequence of this different atomic arrangement, the XANES spectra also are different.

4.3. The Ce valence

The question is now that of how to interpret the XANES of Ce in Y_2O_3/Ce-impl. A FEFF calculation is not adequate: the ground state in CeO_2, which is a mixture of multi-electron configurations resulting from a strong hybridization between the oxygen 2p and the Ce 4f orbitals [19], is not taken into account. Hence another approach is necessary. The Anderson impurity model takes into account hybridization between localized states such as d and f states and the valence band of the matrix in which the impurity has been introduced [20]. Recently, Jollet *et al* [21] checked the influence of the valence band shape and of the 5d band shape, which allows one to model the crystal field, on the L_3 x-ray absorption coefficient calculated for a Ce impurity in several oxide matrices. They showed that the band shapes significantly modify the absorption coefficient features near the edge. They performed a pure Ce^{4+} calculation and a pure Ce^{3+} calculation, that led to spectra different from the experimental one. It was not possible with one set of parameters to reproduce the experimental spectrum for a purely trivalent or a purely tetravalent state. In order to reproduce it, it was necessary to mix the calculated spectra for the Ce^{4+} and Ce^{3+} L_3 edges in the proportion 40% Ce^{4+} and 60% Ce^{3+}. A consequence of this result is that the implanted Ce ions must be at two sites, one corresponding to the Ce^{3+} state, and the other corresponding to the Ce^{4+} state. Such sites are correlated with Ce–O distances of 0.257 nm and 0.232 nm respectively (see table 1). Hence, the expected measured Ce–O distance should be 0.247 nm, in disagreement with the EXAFS result which gives only 0.235 nm, a difference beyond the experimental uncertainty.

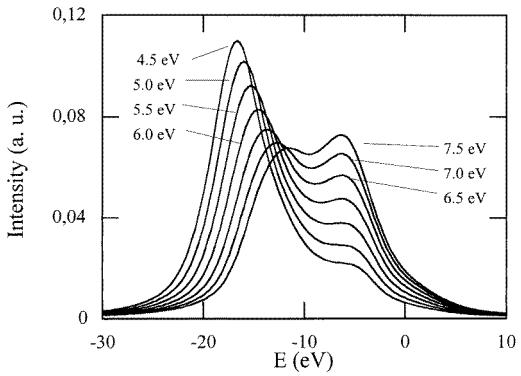

Figure 4. Ce^{4+} L_3 edges calculated for different Δ values with the following parameters: the Coulomb interaction between 4f electrons $U = 10.5$ eV, the exchange interaction between 4f electrons $J = 0$, the f-electron–core-hole interaction $U_{fc} = 12.5$ eV, the f-electron–d-electron interaction $U_{fd} = 4$ eV, the d-electron–core-hole interaction $U_{dc} = 5$ eV, and the hybridization between f electrons and the valence band $V = 0.76$ eV. The shape of the valence band is a crenel 14 eV wide, and the shape of the 5d band is a crenel 6 eV wide.

Therefore we performed a new calculation: we started from the Ce^{4+} state, the closest one in terms of Ce–O distance, and varied the quantity $\Delta = E_f - E_{v0}$ where E_{v0} is the energy of the centre of the valence band. In doing that, we assumed that there is a charge transfer between the f state and the valence band which is monitored by the Δ parameter. The evolution of the spectrum with the Δ parameter is shown in figure 4. For a Δ value of 5.5 eV, a calculated shape close to the experimental one is found. This supports our assumption of a Ce ion with an intermediate charge state resulting from the interaction of the f state with the valence band of Y_2O_3.

5. Conclusions

Ce has been implanted in Y_2O_3. The interpretation of the Fourier transform taken from the oscillations of the absorption coefficient allowed us to conclude that Ce occupies the Y site. The structural information concerning the Ce site is well provided by combining a FEFF calculation and a simulation of the oscillation corresponding to the first O shell around Ce. This substitution should lead to a trivalent oxidation state for Ce.

However, the XANES features are different from those for purely trivalent Ce. The Anderson impurity model, as it was used here, i.e. with ingredients which take into account actual electronic and crystallographic parameters, is needed to interpret the near-edge features. Two possible interpretations of these features are thus provided. The XANES features can be thus interpreted either as due to 40% Ce^{4+} and 60% Ce^{3+} or to an intermediate charge state resulting from the interaction of the f state with the actual valence band of Y_2O_3. The first interpretation is ruled out using the simple argument that the EXAFS result is incompatible with a two-site occupancy corresponding to two different Ce–O distances. Hence it is the coupling of the XANES and EXAFS interpretations which provides us with a more precise description of the Ce state in Y_2O_3.

Acknowledgments

We thank G Vlaic for checking the absence of harmonics at 5700 eV. We are grateful to the technical staff concerned with the implantors of the Centre de Spectrométrie Nucléaire et de Spectrométrie de Masse for their help during the implantations and RBS measurements. W Felsch is acknowledged for providing us with the Ce/Fe layered sample and M J Guittet for the experimental result on the yttria valence band. We also wish to acknowledge V Briois and G Krill from LURE for fruitful discussions.

References

[1] Borowski M, Traverse A and Dallas J P 1995 *J. Mater. Res.* **10** 3136
[2] Brandes E A (ed) 1983 *Smithells Metals Reference Book* 6th edn (London: Butterworth)
[3] Traverse A, Parent P, Mimault J, Hagège S and Du J 1994 *Nucl. Instrum. Methods* B **84** 204
[4] Griscom D L, Krebs J J, Perez A and Treilleux M 1992 *Nucl. Instrum. Methods* B **32** 272
[5] McHargue C J, Sklad P S, McCallum J C, White C W, Perez A and Marest G 1990 *Nucl. Instrum. Methods* B **46** 144
[6] Jollet F, Noguera C, Thromat N, Gautier M and Duraud J P 1992 *Phys. Scr.* **41** 251
Jollet F, Noguera C, Thromat N, Gautier M and Duraud J P 1990 *Phys. Rev.* B **42** 7587
Ching W Y and Xu Y N 1990 *Phys. Rev. Lett.* **67** 835
[7] Traverse A, Parent P, Mimault J, Thromat N, Gautier M, Duraud J P, Flank A M, Quivy A and Fontaine A 1994 *Nucl. Instrum. Methods* B **86** 270
[8] Douillard L, Gautier M, Thromat N, Henriot M, Guittet M J, Duraud J P and Tourillon G 1994 *Phys. Rev.* B **49** 16 171
[9] Chaumont J, Lalu F, Salomé M and Lamoise A M 1981 *Nucl. Instrum. Methods* **189** 193
[10] Ziegler J F, Biersack J P and Littmark U 1986 *The Stopping and Range of Ions in Solids* vols 1 and 2 (New York: Pergamon)
[11] Bernas H, Chaumont J, Cottereau E, Meunier R, Traverse A, Clerc C, Kaitasov O, Lalu F, Le Du D, Moroy G and Salomé M 1992 *Nucl. Instrum. Methods* B **62** 416
[12] Michalowizc A 1991 *Logiciels pour la Chimie* vol 102 (Paris: Société Française de Chimie)
[13] Rehr J J, Mustre de Leon J, Zabinski S I and Albers R C 1991 *J. Am. Chem. Soc.* **113** 5135
[14] Al Karaghouli A R 1970 *Chem. Commun.* 135
[15] Doolittle L R 1986 *Nucl. Instrum. Methods* B **15** 227
[16] Bianconi A, Marcelli A, Dexpert H, Karnatak R, Kotani A, Jo T and Petiau J 1987 *Phys. Rev.* B **35** 806

[17] Donnet C, Marest G, Montcoffre N, Jousset J, Rahioui A, Esnouf C and Brunel M 1991 *Nucl. Instrum. Methods* B **50–60** 1205
[18] Du J, Traverse A and Hagège S 1993 *Mater. Sci. Forum* **126–128** 703
[19] Kotani A and Ogasawara H 1992 *J. Electron. Spectrosc. Relat. Phenom.* **60** 257
[20] Anderson P W 1961 *Phys. Rev.* **124** 41
Gunnarsson O and Schönhammer K 1983 *Phys. Rev.* B **28** 4315
[21] Jollet F, Ortiz V and Crocombette J P 1997 *J. Electron Spectrosc. Relat. Phenom.* **86** 83